Effects of tree morphometry on net snow cover radiation on forest floor for varying vegetation densities

Bijan Seyednasrollah[1] and Mukesh Kumar[1]

[1]   Using a forest radiation model, this paper explores the effects of tree morphometric parameters and shape on net snow cover radiation on the forest floor. Results show that tree shape, height and crown size and density have significant effects on the amount of radiation on forest floor and its variation with vegetation density. In clear sky conditions, where net radiation frequently shows a nonmonotonic decreasing then increasing trend with increasing vegetation density, a smaller radiation minimum is obtained for taller trees, larger and denser crowns, and cylindrical-shaped crowns. The obtained radiation minimum is also expressed at a smaller vegetation density for these tree configurations. In contrast, trees with smaller crown dimensions show propensity for a monotonically decreasing trend in net radiation with increasing vegetation density. The sensitivity to tree morphometric parameters, especially tree height and crown width and density, on forest floor radiation are however relatively modest for interspersed cloudy conditions. The results will facilitate identification of forest management strategies to minimize or maximize net radiation in snow-dominated forested watersheds and will allow intercomparison of snowmelt rates between forests with different vegetation densities and morphological characteristics.

Citation: Seyednasrollah, B., and M. Kumar (2013), Effects of tree morphometry on net snow cover radiation on forest floor for varying vegetation densities, *J. Geophys. Res. Atmos.*, *118*, doi:10.1002/2012JD019378.

1. Introduction

[2] In snow-dominated forested watersheds, radiation is the primary control on snowmelt. In order to predict the timing and amount of snowmelt, quantification of net snow cover radiation on the forest floor (NSRF) is important. One of the controls on NSRF is vegetation density in forests. Knowledge of variation in NSRF with vegetation density can potentially be used to modulate NSRF using forest management strategies such as stocking and thinning. Vegetation densities that result in minimization of NSRF can lead to reduction in snowmelt rates, which in turn may promote moderation of peak flows and availability of melt recharge until late in the season. This may in turn be used to potentially manage the magnitude and timing of snowmelt discharge from forested watersheds. It is to be noted, however, that since canopy structure controls light availability of understory ecosystems [*Chavez and Macdonald*, 2010; *Hanson and Lorimer*, 2007], any forest management practice should be performed only after trade-offs across all the interlinked systems have been accounted for. Many efforts have explored how changes in vegetation density may influence net radiation on the forest floor [*Bohren and Thorud*, 1973; *Hardy et al.*, 1997; *Reifsnyder and Lull*, 1965; *Seyednasrollah et al.*, 2013; *Sicart et al.*, 2004]. Disparate relationships between snow-covered forest floor radiation to average spacing between trees or vegetation density have been reported. In the boreal forest at ~54°N latitude, net radiation and snowmelt rates were observed to be insensitive or sometimes increasing for higher vegetation densities [*Price and Dunne*, 1976]. Due to increasing longwave and decreasing shortwave radiation components with increasing vegetation density, incoming net radiation in a lodgepole pine forest at ~39°N latitude was observed to have a minimum for an intermediate vegetation density [*United States Army Corps of Engineers*, 1956]. In white spruce (*Picea glauca*) forests in Maine at ~45°N latitude, a minima in radiation (NSRF$_{min}$) was predicted at an intermediate vegetation density with 40% canopy closure [*Seyednasrollah et al.*, 2013]. Similar results have been reported for pine forests in Oregon, ~45°N latitude [*Reifsnyder and Lull*, 1965]. The distinct relationships between NSRF and vegetation density at different locations can be attributed to multiple factors, including (a) topographic setting (e.g., aspect and slope) of the site, (b) latitudinal controls on extraterrestrial radiation, (c) climatological characterisitics, (d) snowpack characterstics (e.g., snow surface temperature and albedo), and (e) tree morphometry. Effects of topographic setting and sky cover on the relation between NSRF and vegetation density [*Seyednasrollah et al.*, 2013] and of climatological characteristics on radiation [*Lundquist et al.*, 2013] have been previously explored.

[3] This research focuses on how different tree morphometry parameters such as tree height, canopy shape, radius, depth,

[1]Nicholas School of the Environment, Duke University, Durham, North Carolina, USA.

Corresponding author: M. Kumar, Nicholas School of the Environment, Duke University, PO Box 90328, Durham, NC 27708, USA. (mukesh.kumar@duke.edu)

and density may affect net radiation on the forest floor and its variation with vegetation density. Of particular interest is the understanding of how variations in tree morphometric parameters influence the vegetation density at which radiation is minimum. Since most of the parameters considered here, including canopy coverage [*Gaulton and Malthus*, 2010; *Lee and Lucas*, 2007], height [*Breidenbach et al.*, 2008; *Falkowski et al.*, 2006; *Gatziolis et al.*, 2010; *Lee and Lucas*, 2007; *Pascual et al.*, 2010] and crown dimensions [*Anjin et al.*, 2012; *Falkowski et al.*, 2006; *Riano et al.*, 2004], shape [*Kato et al.*, 2009; *Oshio et al.*, 2012], and density [*Cao and Dean*, 2011; *Hosoi and Omasa*, 2012; *Riano et al.*, 2004] are all obtainable from light detection and ranging (lidar) data, the results can be used by forest managers for evaluation of the sensitivity and influence of tree morphometic parameters on net radiation reaching the forest floor at watershed scales.

2. Approach

2.1. Modeling the Influence of Tree Morphometry on Snow-Covered Forest Floor Radiation

[4] This research utilizes the forest radiation model (FoRM) [*Seyednasrollah et al.*, 2013] to analyze how tree heights and crown shape, radius, depth, and density influence NSRF. For simplicity, FoRM is applied on a snow-covered forest with homogeneously gridded tree distribution; however, the model formulation is generic enough to be applied for NSRF calculations within heterogeneous forest patches. To evaluate how morphometric characteristics influence NSRF for changing vegetation density, the distance between trees, d, is varied between experiments. Averaged NSRF is calculated from winter solstice ($t1$) to summer solstice ($t2$) on the unit rectangular area (A) using

$$\text{NSRF} \quad = \quad \frac{\int_{t1}^{t2}\int_A R_{\text{Net}}\, dA\, \mathrm{d}t}{(t2 \; - \; t1)A} \tag{1}$$

where R_{Net} is net radiation flux on the forest floor. The solstice to solstice period is considered for evaluation of NSRF as it conservatively overspreads the entire range of interannual variability throughout the snow season. It is to be noted that the NSRF formulation is generic and applicable for any place- and year-specific snow cover duration. R_{Net} in equation (1) is calculated using

$$R_{\text{Net}} \quad = \quad \downarrow L_{\text{sky}} \; + \; \downarrow L_{\text{crown}} \; + \; \downarrow L_{\text{trunk}} \; - \; \uparrow L_{\text{snow}}$$
$$+ \; \downarrow S_{\text{dir}} \; + \; \downarrow S_{\text{dif}} \; - \; \uparrow S_{\text{snow}} \tag{2}$$

where $\downarrow L_{\text{sky}}, \downarrow L_{\text{crown}}$, and $\downarrow L_{\text{trunk}}$ are incoming longwave emissions from sky, tree crown, and trunk, respectively, $\uparrow L_{\text{snow}}$ is emitted longwave radiation from snow on the forest floor, $\downarrow S_{\text{dir}}$ and $\downarrow S_{\text{dif}}$ are incoming direct and diffuse shortwave radiation components, and $\uparrow S_{\text{snow}}$ is reflected shortwave radiation from snow. To aid analyses, R_{Net} can be expressed as the sum of net longwave (L_{Net}) and shortwave (S_{Net}) radiation components, where L_{Net} and S_{Net} are defined as

$$L_{\text{Net}} \quad = \quad \downarrow L_{\text{sky}} \; + \; \downarrow L_{\text{crown}} \; + \; \downarrow L_{\text{trunk}} \; - \; \uparrow L_{\text{snow}} \tag{3}$$

$$S_{\text{Net}} \quad = \quad \downarrow S_{\text{dir}} \; + \; \downarrow S_{\text{dif}} \; - \; \uparrow S_{\text{snow}} \tag{4}$$

[5] Readers are referred to *Seyednasrollah et al.* [2013] for more information about evaluation and validation of

radiation components. Relevant equations are briefly presented in Appendix A. The magnitude and temporal variation of individual radiation components, and consequently the NSRF, are impacted by tree morphometry in the following two ways: (a) by influencing the viewable fraction of hemispherical sky (SVF) and (b) by affecting the length of radiation beam inside the crown structure (L_{path}). Changes in sky view factor (SVF) proportionally influence $\downarrow L_{\text{sky}}$ and $\downarrow S_{\text{dif}}$, while longwave radiation from the tree ($\downarrow L_{\text{tree}} = \downarrow L_{\text{crown}} + \downarrow L_{\text{trunk}}$) is conversely affected by it (see equations (A2), (A3), and (A6)). On the other hand, an increase in path length, L_{path}, leads to increase in shading fraction (SF, the shaded portion of the forest floor), which in turn results in a decline in $\downarrow S_{\text{dir}}$. $\uparrow S_{\text{snow}}$ is dependent both on SVF and L_{path} but it is dominantly influenced by L_{path}. This is because $\uparrow S_{\text{snow}}$ is mainly affected by $\downarrow S_{\text{dir}}$, which in turn is dependent on L_{path} (see equation (A5)). $\uparrow L_{\text{snow}}$ is independent of SVF and L_{path} (see equation (A4)). Since individual radiation components, and hence the NSRF, are affected both by SVF and L_{path}, the variation of NSRF for different vegetation densities is expected to change with tree morphometry. To evaluate the effects of different tree morphometric configurations on individual energy components, SVF and L_{path} are calculated for a range of tree morphometric characteristics.

2.2. Evaluation of SVF and L_{path}

[6] A ray tracing method is used to estimateSVF and L_{path}. Sky view factor is quantified by the *SkyMap* algorithm [*Seyednasrollah et al.*, 2013], which calculates the probabilistic viewable fraction of hemispherical sky at a given point using

$$\text{SVF} \quad = \quad \int_0^{2\pi}\int_\gamma^{\frac{\pi}{2}} \frac{p(\omega, \varphi)}{\pi^2}\, \mathrm{d}\omega \mathrm{d}\varphi \tag{5}$$

$$\gamma = \begin{cases} \sec^{-1}\left(\sqrt{1 \; + \; \cos^2\varphi \tan^2\beta}\right) & \text{for } \frac{\pi}{2} \leq \varphi \leq 3\frac{\pi}{2} \\ -\sec^{-1}\left(\sqrt{1 \; + \; \cos^2\varphi \tan^2\beta}\right) & \text{otherwise} \end{cases} \tag{6}$$

where φ and ω are azimuthal and altitudinal angles, γ is directional horizon angle, and $p(\omega, \varphi)$ is the probability that sky is visible along φ and ω directions. $p(\omega, \varphi)$ is obtained by

$$p(\omega, \varphi) \quad = \quad e^{-G\,\lambda\,L_{\text{path}}(\omega, \varphi)} \tag{7}$$

where G is the projection coefficient of leaf orientation (dimensionless), λ is the effective foliage density (m^{-1}), and $L_{\text{path}}(\omega, \varphi)$ is the length of a radiation beam passing through the canopy (m). Path length, which varies temporally, is calculated using a ray tracing method similar to the one discussed in *Essery et al.* [2008], where path length calculations were performed for an ellipsoidal crown shape for a level site. Here, the formulation is extended to account for inclined topography with any given aspect and for other tree crown shapes (cylindrical and conical). $L_{\text{path}}(\omega, \varphi)$ is sum of path lengths through all crowns ($L_{\text{path},1}(\omega, \varphi)$) along a ray's path:

$$L_{\text{path}}(\omega, \varphi) \quad = \quad \sum_{\text{multiple trees}} L_{\text{path},1}(\omega, \varphi) \tag{8}$$

[7] Notably, ω and φ at any instant are equal to solar altitude (α) and azimuth angles (Z), respectively; $L_{\text{path},1}$'s for three different crown shapes on a forested hillslope with an inclination of β and an orientation (azimuth) of Z_s from

Cylindrical	Ellipsoidal	Conical
Equation defining tree crown		
$\dfrac{(x - x_t)^2 + (y - y_t)^2}{R_c^2} = 1$	$\dfrac{(x - x_t)^2 + (y - y_t)^2}{R_c^2} + \dfrac{(z - H + D_C/2)^2}{(D_C/2)^2} = 1$	$\dfrac{(x - x_t)^2 + (y - y_t)^2}{(R_C/D_C)^2} = (z - H)^2$
Ray trace equation		
	$\begin{cases} x = x_s + l \cos\alpha \sin(Z - Z_s) \\ y = y_s - l \cos\alpha \cos(Z - Z_s) \\ z = z_s + l \sin\alpha \end{cases}$	

Figure 1. Ray trace equations for cylindrical, ellipsoidal, and conical crowns. Here H is tree height, R_c is crown radius, D_c is crown depth, α is solar altitude angle, Z is solar azimuth angle, β is hillslope angle, Z_s is the hillslope aspect, and d is distance between trees.

the principal south direction are calculated using a ray tracing method. This involves solving for intersection coordinates using equations defining a tree crown and the ray trace as shown in Figure 1. The path length through a single tree, $L_{path,1}$, is the difference between two positive solutions of the quadratic equation:

$$al^2 + bl + c = 0 \qquad (9)$$

where l is the length along the ray trace, and a, b, and c are coefficients calculated based on Table 1. L_{path} is calculated as

$$L_{path,1} = \begin{cases} \dfrac{\sqrt{\Delta}}{a} & \Delta > 0 \\ 0 & \Delta \leq 0 \end{cases} \qquad (10)$$

$$\Delta = b^2 - 4ac \qquad (11)$$

[8] For open sky, $L_{path} = 0$ for all sky directions (ω, φ), resulting in $p = 1$. Using L_{path} from equation (8), the canopy transmissivity (τ) and the shading fraction (SF) are calculated as

$$\tau = \frac{\int_A e^{-G \lambda L_{path}(\omega, \varphi)} \, dA}{A} \qquad (12)$$

$$SF = \frac{\int_A \sigma \, dA}{A}, \text{where } \sigma = \begin{cases} 1 & \text{if } L_{path}(\omega, \varphi) > 0 \\ 0 & \text{if } L_{path}(\omega, \varphi) = 0 \end{cases} \qquad (13)$$

[9] The full description of path length and sky view factor calculations is presented in *Seyednasrollah et al.* [2013].

2.3. Data and Experiment Setup

[10] Five experiments were conducted to aid the understanding of how tree morphometric parameters affect NSRF on the forest floor and its variation with vegetation density. The experiments were performed for a white spruce (*Picea glauca*) [*Gilman and Watson*, 1994] forest stand near Greenville, ME (45.45°N). The species represents a relatively common conifer tree that is widely distributed in Northern Hemisphere forests that extend from 43° (Maine) to 69° north latitude (Alaska) [*Maine Forest Commissioner*, 1908; *plantmaps.com*, 2012] and hence was selected as a generic conifer for these investigations. To some extent, the site can be considered as a representative of other midlatitude North American snow-dominated forests that has summoned considerable interest in understanding the effects of coniferous forest densities on seasonal snow energetics. White spruce has a cylindrical crown shape and can grow up to 28 m in height and 6 m in width [*Arbor Day Foundation*, 2012; *Maine Forest Commissioner*, 1908]. Starting from a representative configuration of white spruce trees (Table 2) which was considered as the base configuration for all following experiments, FoRM was run for three different tree shapes and for a range of tree height and crown radius, depth, and density. In each experiment, only one of the morphometric parameters was modified to assess the influence of parameters in isolation. In experiment 1 (section 3.1), the three most common shapes of tree crowns were considered: cylindrical, ellipsoidal, and conical. In addition to white spruce (*Picea glauca*) trees, cylindrical shape is exhibited by crowns of species such as eastern red cedar (*Juniperus virginiana*), Colorado blue spruce (*Picea pungens*), and Leyland cypress (*Cupressus leylandii*). Ellipsoidal crown shapes are observed for many species including white pine (*Pinus strobus*) and Scots pine (*Pinus sylvestris*). Tree species such as balsam fir (*Abies balsamea*), Canadian hemlock (*Tsuga canadensis*), Norway spruce (*Picea abies*), Black Hills spruce (*Picea glauca var. densata*), and mugo pine (*Pinus mugo*) have conical-shaped crowns [*Arbor Day Foundation*, 2012]. In experiment 2 (section 3.2), NSRF was simulated for three tree heights ranging from 18 to 30 m.

Table 1. Explanation of Ray Trace Equation Coefficients

Cylindrical

$$a = \frac{\cos^2\alpha}{R_C^2}$$

$$b = \frac{2\cos\alpha(\cos(Z - Z_S)(y_t - y_s) + (x_s - x_t)\sin(Z - Z_S))}{R_C^2}$$

$$c = \frac{-R_C^2 + (x_s - x_t)^2 + y_t^2 + y_s(-2y_t + y_s)}{R_C^2}$$

Ellipsoidal

$$a = \frac{R_C^2 + (D_C/2)^2 + \left(-R_C^2 + (D_C/2)^2\right)\cos(2\alpha)}{0.5R_C^2D_C^2}$$

$$b = \frac{8\left((D_C/2)^2\cos(Z - Z_S)\cos\alpha(y_t - y_s) + (D_C/2)^2(x_s - x_t)\cos\alpha\,\sin(Z - Z_S) + R_C^2\sin\alpha(-H + D_C/2 + z_s)\right)}{R_C^2D_C^2}$$

$$c = -1 + \frac{(x_s - x_t)^2 + y_t^2 + y_s(-2y_t + y_s)}{R_C^2} + \frac{4(-H + D_C/2 + z_s)^2}{D_C^2}$$

Conical

$$a = \frac{D_C^2\cos^2\alpha}{R_C^2} - \sin^2\alpha$$

$$b = \frac{2D_C^2\cos\alpha(\cos(Z - Z_S)(y_t - y_s) + (x_s - x_t)\sin(Z - Z_S))}{R_C^2} + 2H\sin\alpha - 2z_s\sin\alpha$$

$$c = -H^2 + \frac{D_C^2\left((x_s - x_t)^2 + y_t^2 + y_s(-2y_t + y_s)\right)}{R_C^2} + 2Hz_s - z_s^2$$

For cylindrical-shaped trees, the considered height range is representative for white spruce (*Picea glauca*), Colorado blue spruce (*Picea pungens*) and red cedar (*Juniperus virginiana*) [*Arbor Day Foundation*, 2012]. In experiment 3 (section 3.3), NSRF was modeled for five crown radii ranging from $R_C = 1.5$ to 4.5 m. The range is representative of many tree species with cylindrical-shaped crowns, with red cedar (*Juniperus virginiana*) being at the lower range of spectrum ($R_C = 1.5$ to 2.3 m) and blue spruce (*Picea pungens*) being at the higher end ($R_C = 3.8$ to 4.5 m). To evaluate how crown depth (distance between bottom and top of the crown) affects NSRF in relation to vegetation density, in experiment 4 (section 3.4), four different crown depths were considered: $D_C = 6$, 12, 18, and 20 m. For this experiment, tree height was left unchanged. To understand how crown density (λ), which is quantified by the effective foliage density, affects NSRF, FoRM simulations were performed for three crown densities in experiment 5 (section 3.5). Again, all other morphometric parameters were set equal to the base configuration (see Table 2). The climate (air temperature and relative humidity) and observed cloud cover data used in the calculation of radiation components were obtained from National Climatic Data Center (NCDC) [*National Climatic Data Center*, 2012] and National Renewable Energy Laboratory (NREL) [*National Renewable Energy Laboratory*, 2012] stations near Greenville, ME. In all five experiments, vegetation density was quantified as d^{-1}, where d is distance between trees (m). It is to be noted that shortwave and longwave radiation components simulated by FoRM have been previously validated against the observed data, both above and underneath the canopy, in a uniform lodgepole pine forest at the Local Scale Observation Site (LSOS) in Fraser, CO, U. S. (39.9°N, 105.9°W, elevation = 2780 m) [*Seyednasrollah et al.*, 2013]. However, due to lack of net radiation data and its variability with vegetation density for a range of tree heights, crown shapes, sizes, and vegetation densities, the average net radiation values for different tree morphometric parameters presented here remain unvalidated.

3. Results

[11] The results are presented thematically to clearly highlight the effect of individual tree morphometric parameters following the discussions outlined in section 2.3.

3.1. How Does Crown Shape Affect Net Radiation on the Forest Floor?

[12] Changes in crown shapes, from cylindrical to ellipsoidal and conical, were found to influence path length (and hence shading fraction) and sky view factor. For the same tree height (H), crown depth (D_C), and radius (R_C), among the three crown shapes, cylindrical crowns have the largest projected area for nonzenith solar orientation compared to conical and ellipsoidal crowns, resulting in a higher shading fraction and therefore smaller S_{Net} (Figure 2). The figure shows the pattern of shadows as path length maps within a rectangular unit area of a gridded forest at 3:00 P.M. local time. A path length of zero denotes an obstruction-free incidence of solar radiation on the forest floor. Areas with path length greater than zero are likely to be tree shadows. On 20 December, within a unit rectangular grid, shading fraction for cylindrical-shaped crown

Table 2. Morphometry of a Representative White Spruce Tree

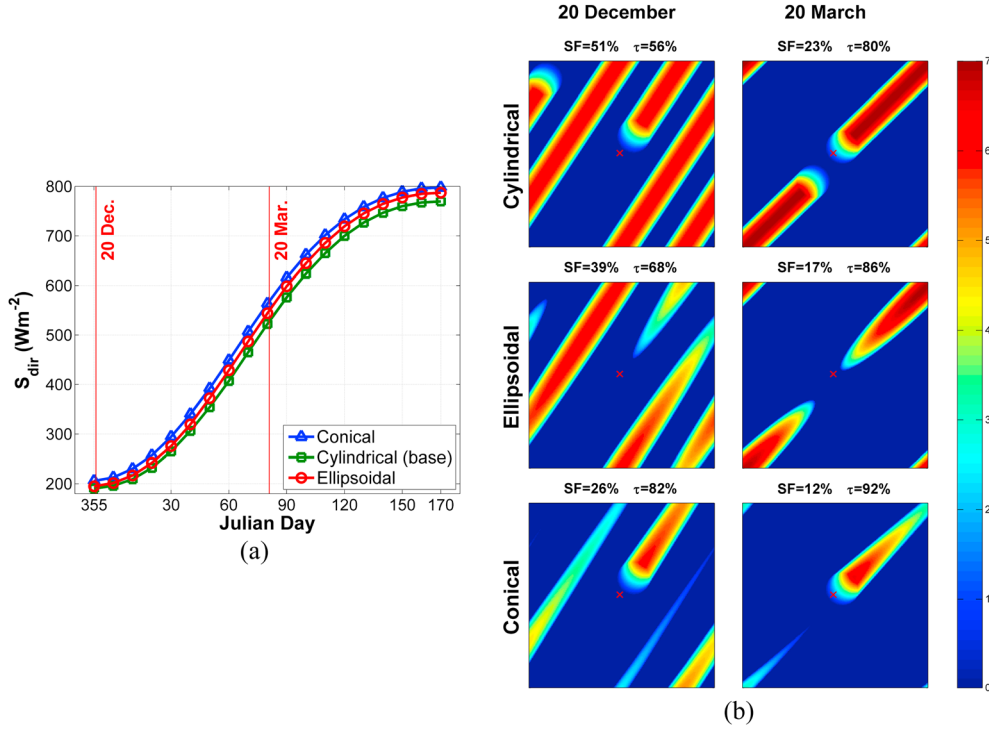| Morphometry Parameter	Symbol	Value or Shape
Crown Shape	-	Cylindrical
Height	H_t	24 m
Crown Radius	$R_{c,t}$	3 m
Crown Depth	$D_{c,t}$	20 m
Crown Density	λ_t	0.99 m^{-1}
Trunk Radius	γ_t	0.4m

Figure 2. (a) Variability of maximum daily direct shortwave radiation between winter and summer solstices for different crown shapes. (b) Path length map at 3:00 P.M. on 20 December and 20 March in forests with cylindrical-, ellipsoidal-, and conical-shaped tree crowns. Trunk path length has not been plotted. Vegetation density $(d^{-1}) = 0.03\,\mathrm{m}^{-1}$. τ represents canopy transmissivity, and SF represents shading fraction.

forests is about 51%, while for ellipsoidal- and conical-shaped crowns, it is only 39% and 26%, respectively. The corresponding canopy transmissivities (τ) for these three crown shapes at 3:00 P.M. local time were observed to be about 56%, 68%, and 82%, respectively. With increasing solar altitude angle later during the snow season, $\downarrow S_{\mathrm{dir}}$ experiences an increase for all crown shapes because of increase in open sky direct shortwave radiation and a concomitant decrease in shading fractions due to low zenith angles. At 3:00 P.M. on 20 March, shading fraction in forests with cylindrical-shaped crowns is the largest and is equal to 23% ($\tau = 80\%$). Shading fractions for ellipsoidal and conical crowns are about 17% ($\tau = 86\%$) and 12% ($\tau = 92\%$), respectively. As a result, direct shortwave radiation is the largest for conical-shaped crowns and the smallest for cylindrical-shaped crowns. The trend is consistent throughout the cold season (Figure 2). $\downarrow S_{\mathrm{dif}}$ is also the largest for conical-shaped crowns. This is because blocked hemispherical area of sky is greatest for cylindrical-shaped crowns and smallest for conical-shaped crowns, which translates to a larger SVF for conical crowns (Figure 3a). The third shortwave energy component, $\uparrow S_{\mathrm{snow}}$, which is proportional to the summation of $\downarrow S_{\mathrm{dif}}$ and $\downarrow S_{\mathrm{dir}}$ hence is also the largest for conical crowns. In contrast, because of smaller SVF for cylindrical crowns, $\downarrow L_{\mathrm{sky}}$ is the smallest and $\downarrow L_{\mathrm{tree}}$ is the largest for them. Since canopy has a higher emissivity than clear sky, L_{Net} contribution is largest for cylindrical crowns. It is to be noted that the trend of S_{Net} and L_{Net} with crown shapes remain the same even for interspersed cloudy conditions.

[13] For a snow season with mostly clear sky conditions, as crown shape changes from cylindrical to ellipsoidal and

conical, for vegetation densities ranging from open areas to $d^{-1} \approx 0.13\,\mathrm{m}^{-1}$, the rate of increase in shortwave radiation is greater than the decrease in longwave radiation reaching the floor. As a result, within this range of vegetation density, NSRF was observed to be smallest for trees with cylindrical-shaped crowns and largest for conical crowns (Figure 3c). In very sparse ($d^{-1} < 0.02\,\mathrm{m}^{-1}$; SVF ≈ 1; SF ≈ 0) forests, since both sky view factor and shading fraction are identical for all three crown shapes, NSRF is the same for the three cases. In contrast, SVF and SF are appreciably sensitive to crown shapes at intermediate vegetation densities ($0.03\,\mathrm{m}^{-1} < d^{-1} < 0.13\,\mathrm{m}^{-1}$), resulting in considerable differences in NSRF between the three crown shapes. In very dense forests ($d^{-1} > 0.15\,\mathrm{m}^{-1}$), the variations in SVF and SF for cylindrical and ellipsoidal crown shapes are relatively smaller. At these densities, since shortwave radiation is very small relative to longwave radiation, NSRF generally follows the trend of longwave radiation, which is largest for cylindrical and smallest for conical crowns. Optimum density (d_{min}^{-1}), at which NSRF$_{\mathrm{min}}$ is obtained, increases from cylindrical to ellipsoidal crowns. In fact, the variation of radiation with vegetation density follows a monotonic decreasing trend for conical crowns, and NSRF$_{\mathrm{min}}$ is obtained for very dense forests (Figure 3c).

[14] Relative to the clear sky case, snow season with interspersed clear/cloudy conditions (average sky cloudiness $\approx 56\%$) at Greenville, ME, receives only 61% of above-canopy shortwave radiation (a reduction of about 82 Wm^{-2}) and 110% of above-canopy longwave radiation (an increase of about 22 Wm^{-2}). As a result, magnitude of NSRF in sparse forests
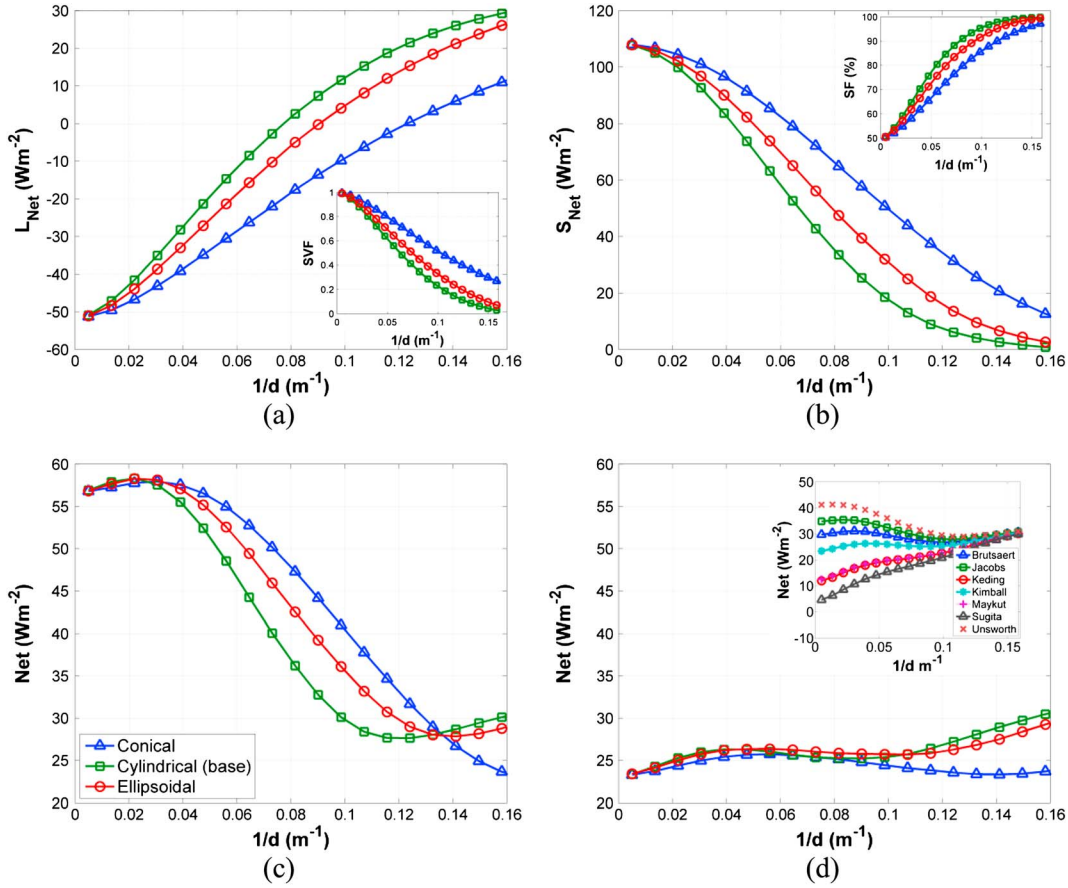
Figure 3. Effect of crown shape on (a) net longwave radiation, (b) net shortwave radiation, (c) net radiation in clear sky conditions, and (d) net radiation in interspersed clear/cloudy sky conditions and sensitivity of NSRF to sky emissivity estimation methods (inset), for a range of vegetation densities. Kimball method has been used as a base model to estimate sky emissivity in cloudy sky conditions.

for interspersed clear/cloudy conditions is much lower than in clear sky conditions (Figure 3d). While the variability of NSRF with vegetation density still shows a local minimum at intermediate vegetation density, the absolute NSRF minimum is obtained in very sparse forests for cylindrical and ellipsoidal crowns and in very dense forests for conical crowns. Notably, for sparser ($d^{-1} < 0.11 m^{-1}$) vegetation densities, the difference in NSRF for the three considered crown shapes is nominal. This is because of almost identical increase and decrease in shortwave and longwave radiations, respectively, as crown shape changes from cylindrical to ellipsoidal and conical. For densities larger than $0.11 m^{-1}$, the increase in longwave radiation for cylindrical and ellipsoidal crowns is larger than the decrease in shortwave radiation. As a result, cylindrical and ellipsoidal crowns express an increasing trend in NSRF for denser forests. In contrast, conical crowns display a decreasing trend in NSRF for denser forests. It is to be noted that all the results presented in this paper, for interspersed cloudy conditions, are based on the method by *Kimball et al.* [1982], which is considered as one of the more reliable models (among Brutsaert, Jacobs, Keding, Maykut, Sugita, Unsworth and Kimball methods) for estimating sky emissivity in cloudy conditions [*Flerchinger et al.*, 2009]. Choice of Kimball method in this paper also explains why NSRF trend with vegetation density is different than the monotonic trend reported in *Seyednasrollah et al.* [2013],

where sky emissivity was estimated using Keding model. Notably, the obtained trends in NSRF are markedly sensitive to choice of algorithms used for estimating sky emissivity in cloudy conditions. Unsworth and Jacobs models generally produce relatively larger sky emissivity values, which in turn results in higher estimates of longwave radiation, especially in sparse forests. This leads to a decreasing trend in NSRF with increasing vegetation density. Sugita, Maykut, and Keding methods, on the other hand, result in a monotonically increasing trend. Not surprisingly, deviations between different methods are larger in sparser forests where $\downarrow L_{sky}$ is the dominant component. In denser forests, sky view factor decreases, and hence, NSRF becomes less sensitive to the cloud correction method (Figure 3d, inset). This indicates that comparisons of NSRF estimates in dense forests are expected to be valid for all sky emissivity evaluation algorithms.

3.2. How Does Tree Height Influence Net Radiation on the Forest Floor in Relation to Vegetation Density?

[15] For a specific vegetation density, taller trees lead to a smaller sky view factor and larger shading fraction. Since L_{Net} varies conversely with sky view factor, and S_{Net} decreases with increasing shading fraction, L_{Net} increases and S_{Net} decreases with increase in tree height. In very sparse forests ($d^{-1} < 0.01 m^{-1}$), SF ≈ 0 and SVF ≈ 1, and in very dense forests ($d^{-1} > 0.15 m^{-1}$), SF≈1 and SVF ≈ 0, for the
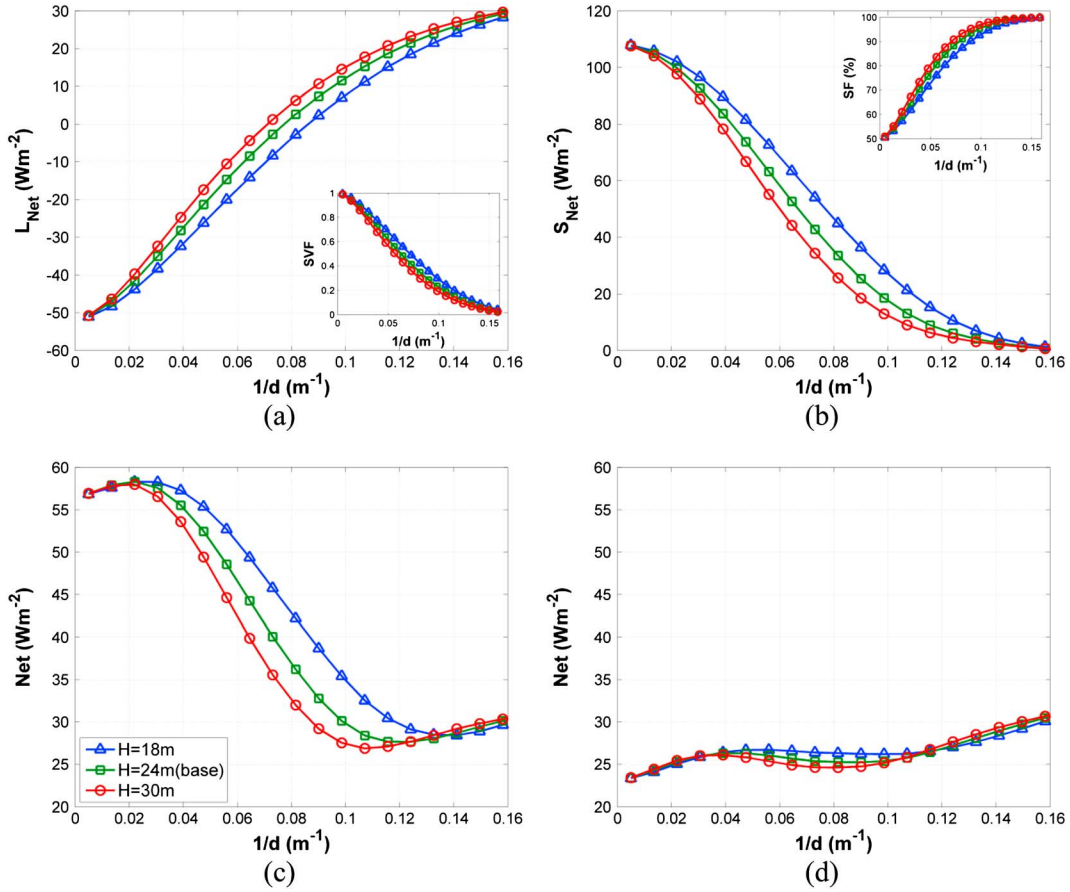
Figure 4. Effect of tree height on (a) net longwave radiation, (b) net shortwave radiation, (c) net radiation in clear sky conditions, and (d) net radiation in interspersed clear/cloudy sky conditions, for a range of vegetation densities.

range of tree heights considered. As a result, both L_{Net} and S_{Net} are independent of the changes in tree height in very sparse and dense forests. At intermediate vegetation densities, with increase in tree height, shading fraction increases and sky view factor decreases, resulting in greater changes in NSRF with tree height. The decrease in net shortwave radiation for intermediate vegetation density is larger than the increase in net longwave for the same density (Figure 4). As a result, NSRF decreases with increasing tree height in relatively sparse ($d^{-1} \approx 0.03 \text{m}^{-1}$) to dense ($d^{-1} \approx 0.13 \text{m}^{-1}$) forests. Because of the larger decrease in S_{Net} than the increase in L_{Net}, NSRF_{min} was obtained at a lower density in forests with taller trees. Furthermore, NSRF_{min} decreases with increasing tree height (Figure 4c). It is to be noted however, that the monotonic shifts in the magnitude of NSRF_{min} and d_{min}^{-1} are specific for the considered location and tree configuration. Their expression in other settings may be quantitatively different based on the magnitude and temporality of individual radiation components, solar elevation angle and air, canopy, and snow temperatures. For interspersed cloudy conditions, the increase in longwave radiation with increase in tree height is negated by the simultaneous decrease in shortwave radiation at all vegetation densities. As a result, NSRF displays very muted sensitivity to tree height, as evident by overlapping NSRF curves in Figure 4d. Notably, NSRF_{min} is always

obtained at very sparse vegetation density for all tree heights considered here.

3.3. How Does Canopy Crown Radius Alter Net Radiation on the Forest Floor?

[16] Changes in crown radius were found to affect both sky view factor and shading fraction. Larger crown radius results in a smaller sky view factor and vice versa. Therefore, L_{Net} increases with increasing R_C. Moreover, L_{path} and SF increase with increasing R_C. Hence, trees with wider crowns result in smaller S_{Net}. For clear sky conditions, the sensitivity of NSRF on crown radius is greater at intermediate vegetation densities in relation to very sparse or dense forests. Since the rate of decrease in S_{Net} is much more than the rate of increase in L_{Net} in sparser forests, and vice versa, NSRF is smaller for wider crowns in sparser forests, and NSRF_{min} is achieved at lower d^{-1} for higher R_C (Figure 5c). In very dense forests ($d^{-1} > 0.15 \text{m}^{-1}$) where the shortwave radiation contribution is small, NSRF is generally larger for wider crowns. However, for dense forests with very narrow crowns (e.g., $R_C = 1.5 \text{ m}$), the contribution of S_{Net} to NSRF can be substantial enough to result in larger NSRF than forests with wider crowns. Consideration of sky cloudiness during the snow season results in a relatively muted sensitivity of NSRF with changing crown radius, especially at intermediate
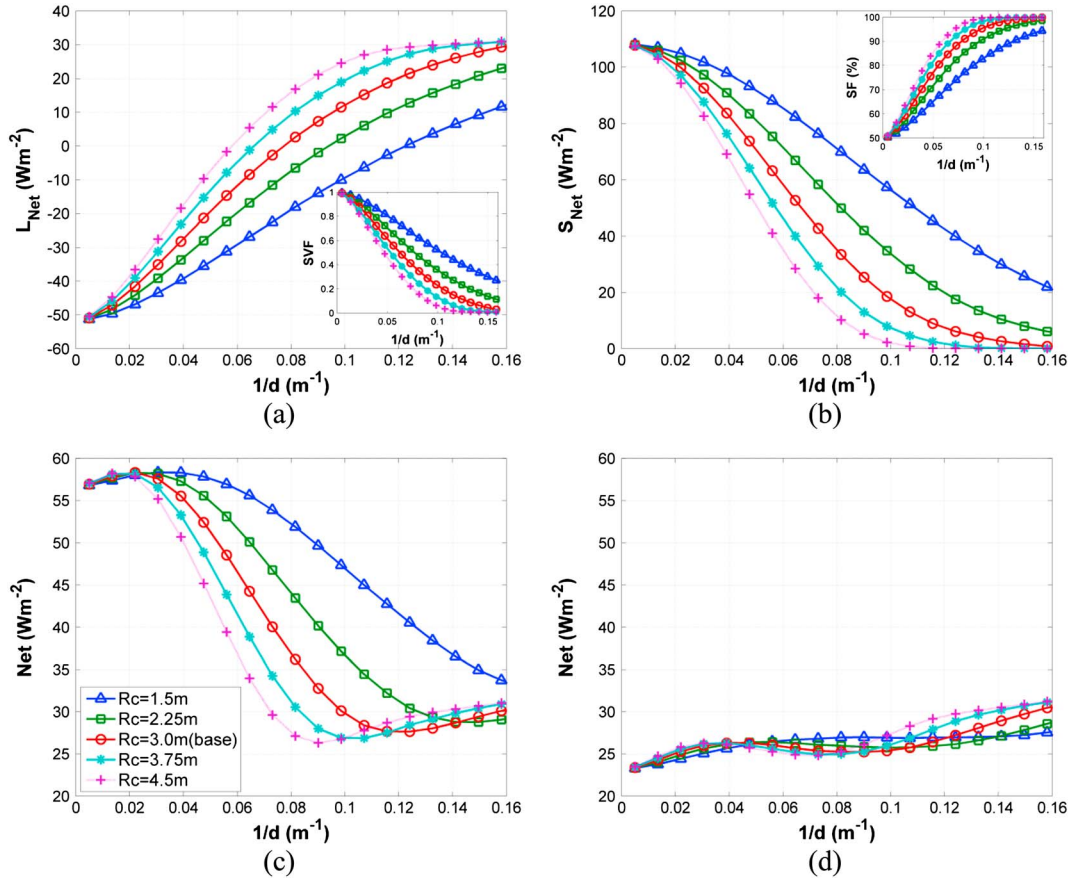
Figure 5. Effect of crown radius on (a) net longwave radiation, (b) net shortwave radiation, (c) net radiation in clear sky conditions, and (d) net radiation in interspersed clear/cloudy sky conditions, for a range of vegetation densities.

densities. This is because of the reduction in rate of change of L_{Net} and S_{Net} with vegetation density for interspersed clear/cloudy sky conditions. It is to be noted that no consistent trend is observed in the variability of NSRF with crown radius. Based on the relative magnitudes of L_{Net} and S_{Net} at different vegetation densities, largest NSRF is obtained for different crown radii. However, in very dense forests ($d^{-1} > 0.15 \text{m}^{-1}$) where the shortwave radiation contribution is small, even more so than in clear sky conditions, NSRF is always larger for wider crowns (Figure 5d). Notably, $NSRF_{min}$ for all considered radii is obtained at very sparse vegetation density.

3.4. How Does Canopy Crown Depth Change Net Radiation Behavior on the Forest Floor?

[17] Crown depths influence both SF and SVF. With increasing crown depth, the hemispherical exposed area of visible sky decreases. As a result, sky view factor decreases, and L_{Net} increases. Changes in L_{Net} with crown depth are larger at intermediate vegetation densities in comparison to very sparse and very dense forests (Figure 6a). Also, shading fraction increases with increasing crown depth, resulting in a smaller S_{Net} (Figure 6b).

[18] For both clear and cloudy sky conditions, the increasing trend of NSRF with vegetation density is insensitive to changes in D_C in sparse forests ($d^{-1} < 0.03 \text{m}^{-1}$). However, in denser forests ($0.03 \text{m}^{-1} < d^{-1}$), NSRF reduces

with increasing D_C for clear sky conditions (Figure 6c). The vegetation density at which radiation is minimum, d_{min}^{-1}, follows a monotonic trend, and it increases for trees with smaller D_C. For trees with small crown depths ($D_C < 6 \text{ m}$), net radiation monotonically decreases with increasing vegetation density. For interspersed cloudy conditions, since the rate of increase in L_{Net} with canopy depth is much more than the decrease in S_{Net}, especially for vegetation density larger than 0.04m^{-1}, NSRF increases with canopy depth (Figure 6d). For denser forests, the sensitivity to D_C is more apparent. It is to be noted that the variability of NSRF with vegetation density still shows a local minimum at intermediate vegetation density (especially for larger D_C). However, the absolute NSRF minimum is obtained in very sparse forests for all the considered canopy depths.

3.5. How Does Crown Density Modulate Net Radiation on the Forest Floor?

[19] As crown foliage density increases, probabilistic interception of radiation (equation (7)), and hence the decay rate of the total incoming radiation flux through canopy increases. Changes in canopy foliage density, λ, influence both L_{Net} and S_{Net} by influencing SVF and SF, respectively. As crown structure becomes denser, less of the sky is viewable through the crown, which leads to a decrease in SVF. As a result, L_{Net} increases with increasing λ because of reduction in SVF
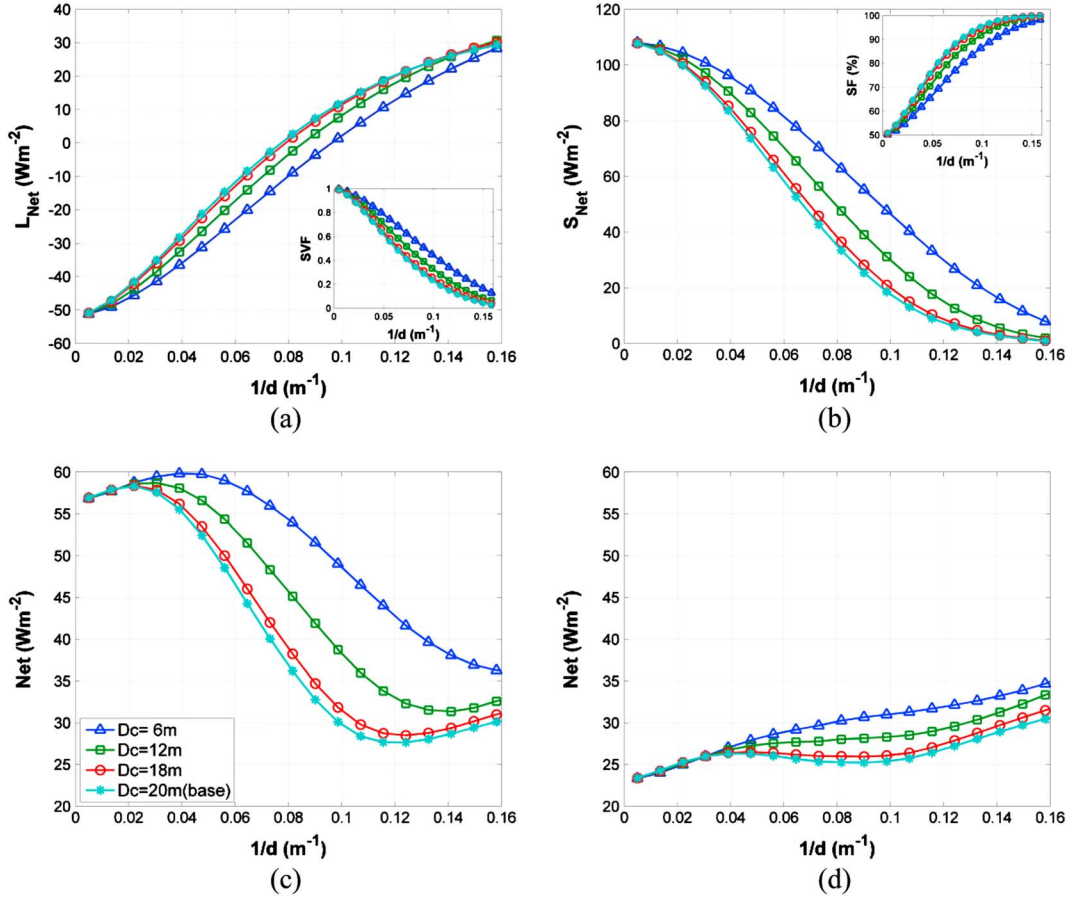
Figure 6. Effect of crown depth on (a) net longwave radiation, (b) net shortwave radiation, (c) net radiation in clear sky conditions, and (d) net radiation in interspersed clear/cloudy sky conditions, for a range of vegetation densities.

(Figure 7a). In contrast, as crown density increases, a smaller amount of shortwave radiation reaches the forest floor, and hence, S_{Net} decreases. With an increase in λ, the decrease in S_{Net} is much more than the rate of increase in L_{Net} (Figure 7b). As a result, for a wide range of vegetation densities ($d^{-1} < 0.13 m^{-1}$) in clear sky conditions, NSRF decreases with increasing crown density. For very dense forests ($d^{-1} > 0.15 m^{-1}$), where S_{Net} is negligible, NSRF experiences a mild increase with increasing λ (Figure 7c). In contrast, changes in S_{Net} and L_{Net} with λ negate each other for interspersed cloudy conditions. As a result, NSRF is almost insensitive to λ (Figure 7d).

4. Synthesis

[20] The results show that forest management strategies such as cutting, thinning, and stocking, which may be used to modulate vegetation density, can be used to alter radiation amount on the forest floor. The effectiveness of these strategies, however, will depend on the tree morphometric characteristics. Further analyses were performed to evaluate parameters that may yield an absolute minimum radiation on the forest floor and to explore the relative influence of individual parameters on NSRF.

4.1. In Search of Absolute Radiation Minima

[21] In order to investigate the tree characteristics for which an absolute radiation minimum may exist, the model was run for a range of combinations of tree configurations (12 m $< D_C < 20$ m, 1.5 m $< R_C < 4.5$ m, and 18 m $< H < 30$ m). In clear sky conditions (Figure 8a), since the minimum radiation decreases with increasing canopy dimensions (see sections 3.1 to 3.5), an absolute radiation minimum (NSRF$_{min} \approx 25 W m^{-2}$) occurs at $d_{min}^{-1} \approx 0.09 m^{-1}$ when $H = 30$ m, $R_C = 4.5$ m, and $D_C = 20$ m. Notably, the absolute radiation minimum is 52% lower than open canopy radiation and 12% lower than radiation for dense forests with base tree configurations. When sky cloudiness is considered (Figure 8b), NSRF$_{min}$ is obtained for an open canopy case.

4.2. Relative Influence of Individual Parameters on Net Radiation

[22] In order to explore the relative role of morphometric parameters (H, R_c, and D_c) on NSRF and d_{min}^{-1}, sensitivity analyses were performed. First, sensitivity of NSRF and d_{min}^{-1} were evaluated for the same percentage change in parameter values (Figures 9a and 9c). With ±20% changes in the parameters, NSRF is observed to be most sensitive to R_c for $0.04 m^{-1} < d^{-1} < 0.11 m^{-1}$ and D_c for $d^{-1} > 0.11 m^{-1}$. NSRF shows the least variations with changes in
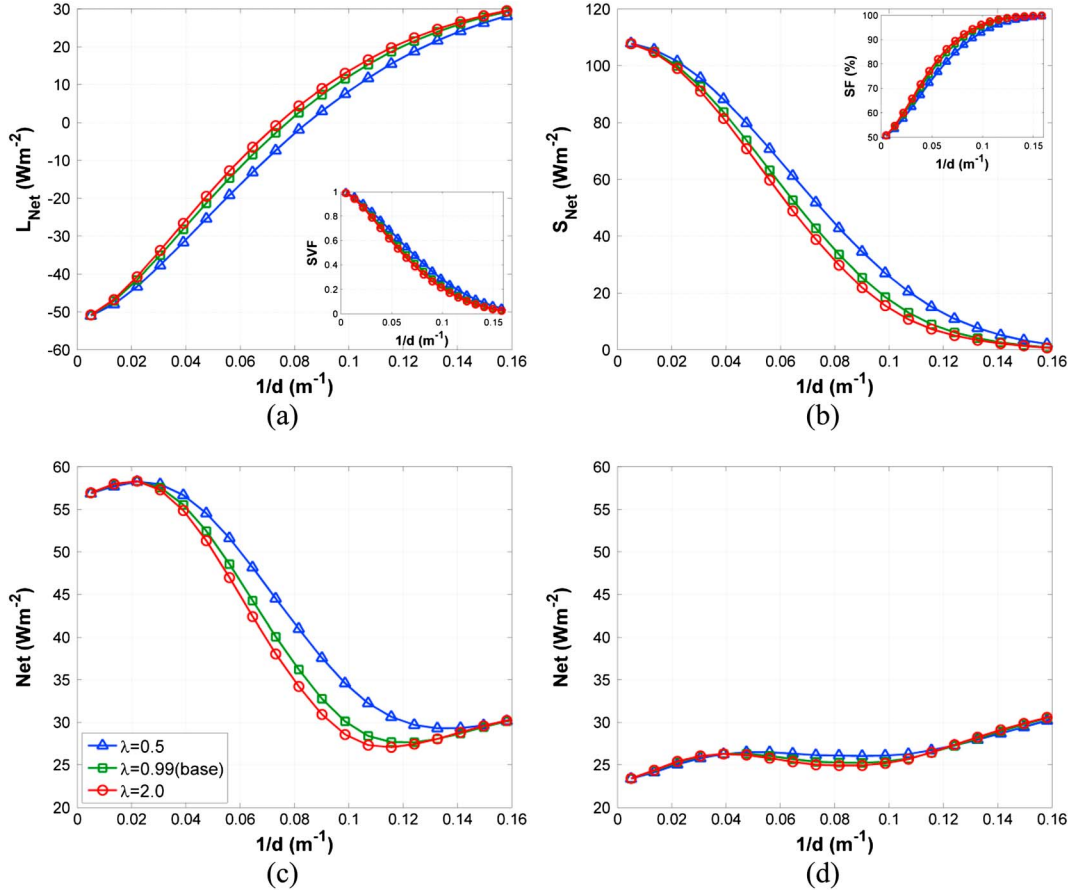
Figure 7. Effect of crown density on (a) net longwave radiation, (b) net shortwave radiation, (c) net radiation in clear sky conditions, and (d) net radiation in interspersed clear/cloudy sky conditions, for a range of vegetation densities.

D_c for $d^{-1} < 0.08 \text{m}^{-1}$ and H for $d^{-1} > 0.08 \text{m}^{-1}$ (Figure 9a). The identification of most sensitive parameters at different vegetation densities can be used to prioritize resources for measurements, as parameters with higher sensitivity should be measured with higher accuracy. Next, variability of NSRF and $d_{\min}^{-1}$ was evaluated for the full range of parameter values

that are typical of white spruce forests (Figures 9b and 9d). The results suggest that H for $d^{-1} < 0.05 \text{m}^{-1}$ and R_c for $d^{-1} > 0.05 \text{m}^{-1}$ play a major role in variability of NSRF. However, NSRF shows very less variability with changes in D_c for $d^{-1} < 0.09 \text{m}^{-1}$ and H for $d^{-1} > 0.09 \text{m}^{-1}$ (Figure 9b). The results highlight that measurement of R_c is
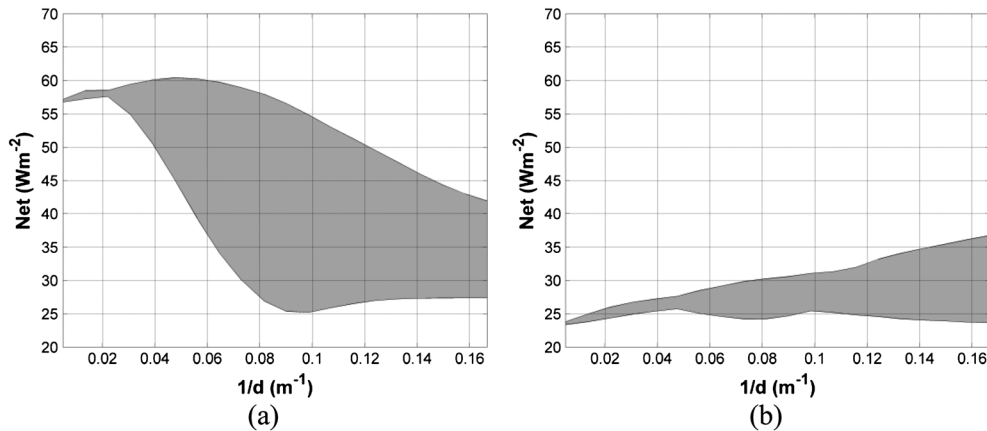

Figure 8. Variability of NSRF with vegetation density for a full range of morphometric parameters for (a) clear and (b) interspersed clear/cloudy sky conditions.
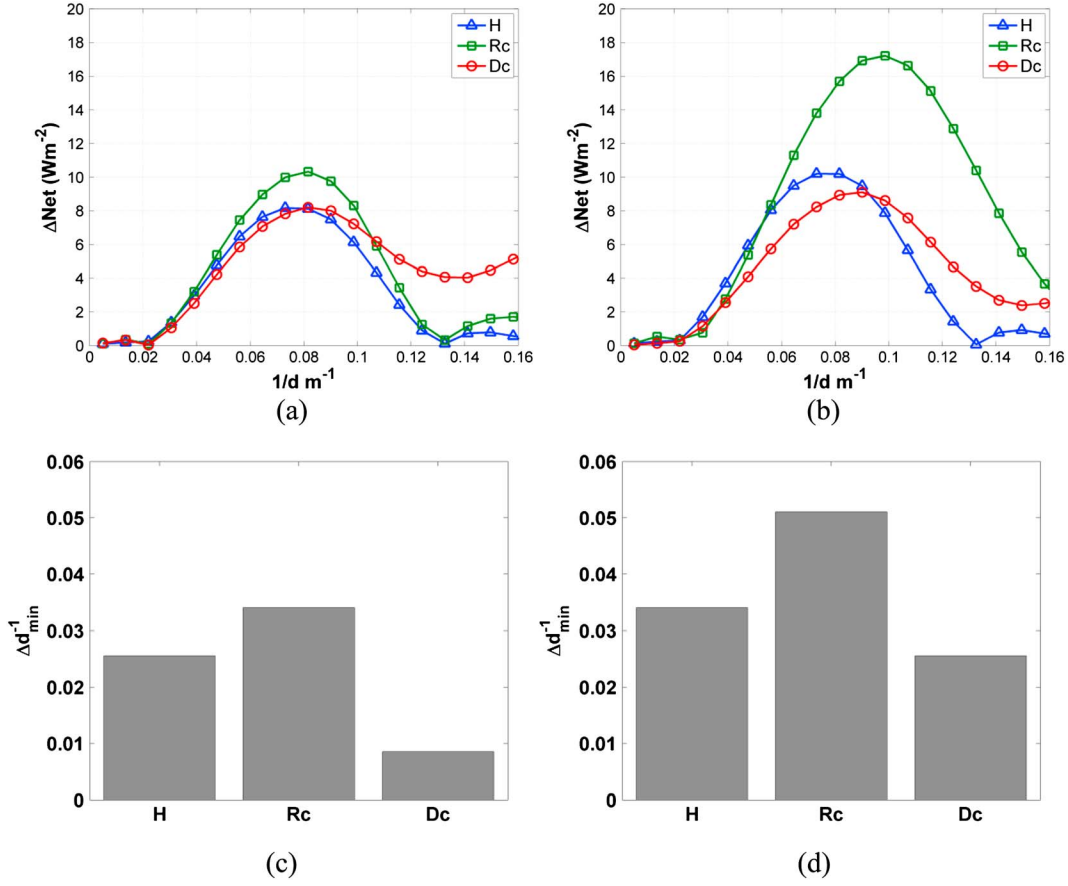
Figure 9. Sensitivity of results to canopy dimensions (tree height H, crown radius R_c, and crown depth D_c). Variation of the net radiation, ΔNet, (a) due to 20% change in each parameter and (b) for the full range of parameter. Variation of optimum density, Δd_{min}^{-1}, (c) due to 20% changes in each parameter and (d) for the full range of parameter, in a white spruce forest.

crucial in order to accurately estimate NSRF in conifer forests. The information can be used to prioritize resources in field campaigns and in development of processing methodologies of lidar data to derive relevant tree morphometric characteristics.

5. Discussion and Conclusions

[23] The research illustrated how tree morphometric characteristics, such as crown shape, tree height, crown radius, crown depth, and crown density, affect net radiation (NSRF) on the forest floor in relation to vegetation density. By changing one morphometry characteristic at a time and keeping the rest unchanged, forest radiation model (FoRM) was used to evaluate the individual effects of tree morphometry characteristics in midlatitude coniferous forests.

[24] Crown shapes affect radiation on the forest floor by modifying the sky view factor and shading fraction, which in turn affects both longwave and shortwave radiation components. For locations with snow seasons composed of mostly clear sky conditions, the optimum density, d_{min}^{-1}, increases from cylindrical- to ellipsoidal- to conical-shaped crowns (Table 3). Hence, the effectiveness of tree cutting practices with a goal to reduce the net radiation on the forest floor will be the most effective at intermediate vegetation density ($d^{-1} \approx 0.12 m^{-1}$) in cylindrical-shaped crowns (e.g., white spruce, eastern red

cedar, Colorado blue spruce, and Leyland cypress), at relatively higher vegetation density ($d^{-1} \approx 0.14 m^{-1}$) in ellipsoidal-shaped crowns (e.g., white pine and Scots pine), and at very high vegetation density ($d^{-1} \approx 0.17 m^{-1}$) for conical-shaped crowns (e.g., balsam fir, Canadian hemlock, Norway spruce, Black Hills spruce, and mugo pine), assuming all other morphometry parameters remain the same. It is to be noted that the results are place specific because of latitudinal controls on extraterrestrial radiation and representative climatology of the site and are valid mostly for mid-latitude forests. For locations with average sky cloudiness > 55% during snow seasons (typical of humid continental climates defined based on Köppen climate classification scheme), forest management practices such as thinning can only have a modest impact on melt timing. Nonetheless, nominal reductions in NSRF can be achieved by managing vegetation density to $d^{-1} \approx 0.07 m^{-1}$ or $d^{-1} < 0.02 m^{-1}$ for cylindrical and ellipsoidal crowns and $d^{-1} < 0.02 m^{-1}$ or $d^{-1} > 0.09 m^{-1}$ for conical crowns.

[25] As tree height increases, NSRF decreases except for very dense forests ($d^{-1} > 0.15 m^{-1}$). In very dense forests, NSRF increases with increasing tree height. Also, the magnitude of $NSRF_{min}$ and d_{min}^{-1} decreases (Table 3). From a forest management perspective, thinning practices in forests with taller trees should yield larger reduction in NSRF than in forests with relatively shorter trees. So modulating stand

Table 3. Effect of Tree Morphometric Characteristics on Net Radiation on Forest Floor for Snow Seasons With Mostly Clear Sky Conditions[a]

	Case Study	$\mathrm{NSRF_{min}}$ (Wm^{-2})	$d_{\min}^{-1}$ (m^{-1})	$\mathrm{NSRF_{max}}$ (Wm^{-2})	$d_{\max}^{-1}$ (m^{-1})	NSRF in Open Areas	NSRF for Very Dense Forests $(d^{-1}>0.16\,m^{-1})$
Crown Shape	Conical	22.9	0.17	58	0.03	56.8	22.9
	Ellipsoidal	27.9	0.14	58.3	0.02	56.8	29.6
	Cylindrical (Base)	27.7	0.12	58.3	0.02	56.9	30.7
Tree Height	$H = 18\,m$	28.4	0.14	58.3	0.02	56.8	30.4
	$H = 24\,m$ (Base)	27.7	0.12	58.3	0.02	56.9	30.7
	$H = 30\,m$	26.9	0.11	58	0.02	56.9	30.9
Crown Radius	$R_C = 1.5\,m$	32.8	0.17	58.3	0.03	56.8	32.8
	$R_C = 2.25\,m$	28.8	0.15	58.3	0.02	56.9	29.6
	$R_C = 3\,m$ (Base)	27.7	0.12	58.3	0.02	56.9	30.7
	$R_C = 3.75\,m$	26.9	0.11	58.2	0.02	57	31.4
	$R_C = 4.5\,m$	26.3	0.09	58.2	0.01	57.1	31.5
Crown Depth	$D_C = 6\,m$	36.2	0.17	59.8	0.04	56.8	36.2
	$D_C = 12\,m$	31.4	0.14	58.7	0.03	56.9	33.5
	$D_C = 18\,m$	28.5	0.12	58.4	0.02	56.9	31.7
	$D_C = 21\,m$ (Base)	27.7	0.12	58.3	0.02	56.9	30.7
Crown Density	$\lambda = 0.5\,m^{-1}$	29.3	0.13	58.3	0.02	56.9	30.7
	$\lambda = 0.99\,m^{-1}$ (Base)	27.7	0.12	58.3	0.02	56.9	30.7
	$\lambda = 2\,m^{-1}$	27.1	0.12	58.3	0.02	57	30.8

[a]Only one morphometric parameter is changed at a time in each case, while others are set equal to the base configuration.

densities in taller forests, e.g., Colorado blue spruce (*Picea pungens*), assuming all other morphometry parameters remain the same, may provide a greater potential to alter snowmelt timing. This is true even for locations with appreciable sky cloudiness during snow seasons. At these locations, thinning may be used to modulate NSRF toward a local radiation minimum, in which case taller forests will again provide a much greater potential to reduce radiation. However, the reduction achieved in this case would be much less than for areas with mostly clear sky conditions. Notably, any forest management intended to achieve absolute NSRF minimum is agnostic of tree height, as it is obtained for a cleared forest.

[26] Changes in crown radius influence both longwave and shortwave net radiations by modifying sky view factor and shading fraction. For locations with snow seasons composed of mostly clear sky conditions, as crown radius increases, $d_{\min}^{-1}$ decreases (Table 3). This highlights the potential of using forest management methods such as tree thinning to modulate net radiation on the forest floor. Moreover, the effectiveness of tree cutting practices for minimization of net radiation (if same number of trees are removed) will be the best for wider trees (e.g., Colorado blue spruce and white spruce) and relatively less effective for narrower crowns (e.g., red cedar), assuming that rest of the geometrical parameters are similar. This is also true for locations with substantial cloudiness during snow seasons. However, the reduction achieved in this case would be much less than for areas with mostly clear sky conditions. Crown depth also affects variations in NSRF. Although NSRF increases with decreasing crown depth, $\mathrm{NSRF_{min}}$ is the smallest for smaller crown depths (Table 3).

[27] Changes in the density of crown markedly affect net radiation on the forest floor. For locations with mostly clear sky conditions during the snow season, net radiation, as well as $\mathrm{NSRF_{min}}$ and $d_{\min}^{-1}$, decreases with increasing crown density (Table 3). This means that trees with higher crown density may offer larger gains in reduction of radiation from tree cutting practices. Again, for locations with considerable cloudiness during snow seasons, the potential reduction that can be achieved is relatively small. It is to be noted that the

results presented in the paper were obtained for flat forests, and they can be expected to be different for other forest floor slopes and aspects. For seasons with mostly clear sky conditions, since $d_{\min}^{-1}$ increases steadily with increasing slope [*Seyednasrollah et al.*, 2013], a decreasing trend followed by an increasing trend in radiation with vegetation density is expected to more likely happen in forests with cylindrical crowns, larger tree heights, and thicker, taller, and denser crowns. In contrast, smaller, shorter, thinner, and sparser crowns will lead to a monotonic decreasing trend in NSRF. Similarly, change in the aspect of a hillslope toward north causes a considerable decrease in S_{Net}, while changes in L_{Net} is only modest [*Seyednasrollah et al.*, 2013]. As a result, $\mathrm{NSRF_{min}}$ is observed at lower vegetation densities. Hence, forests with conical crowns may also, after all, exhibit a decreasing and a subsequently increasing trend in radiation when they are on northerly facing slopes. For forests with ellipsoidal and cylindrical crowns, $\mathrm{NSRF_{min}}$ will be observed at lower vegetation densities. For all radiation results presented in the paper, with increasing slope angle on north facing hillslopes, the decrease in net shortwave radiation is large in relation to modest change in longwave radiation; hence, $d_{\min}^{-1}$ shifts toward lower densities.

[28] It should be highlighted that the trends of net radiation and magnitude of $d_{\min}^{-1}$ presented here are dependent on a wide range of factors including the time period of analysis and representative values of parameters (e.g., snow albedo) used in radiation calculations. We note that a constant average snow albedo was used for the duration of analysis. Accounting for temporal variations in albedo over the whole snow season will influence the outgoing shortwave radiation and hence the NSRF and its variation with density. In the same vein, temporal persistence of intercepted snow cover on a canopy will result in a higher canopy albedo which may lead to enhancement of S_{Net} [*Stahli et al.*, 2009] thus increasing NSRF and $d_{\min}^{-1}$. Despite these considerations, this research clearly indicates how tree morphometry may influence the net radiation and its variability with vegetation density. The presented model could also be combined with

land surface models and lidar-derived data (e.g., tree height and crown shape, size, and density) to enhance our understanding of hydrology of forested watersheds in response to snow accumulation and snowmelt.

Appendix A: Evaluation of Individual Radiation Components

[29] The three longwave energy components from equation (3) are computed using the Stefan–Boltzmann equation [*Gryning et al.*, 2001; *Male and Granger*, 1981; *Marks and Dozier*, 1979; *Pluss and Ohmura*, 1997; *Pomeroy et al.*, 2009; *Sicart et al.*, 2006; *Todhunter et al.*, 1992] as

$$\downarrow L_{crown} \ = \ (1 \ - \ SVF \ - \ TVF) \ \sigma \varepsilon_{can} T_{crown}{}^4 \qquad (A1)$$

$$\downarrow L_{trunk} \ = \ TVF \ \sigma \varepsilon_{can} T_{trunk}{}^4 \qquad (A2)$$

$$\downarrow L_{sky} \ = \ SVF \ \sigma \varepsilon_{sky} T_{air}{}^4 \qquad (A3)$$

$$\uparrow L_{snow} \ = \ \sigma \varepsilon_{snow} T_{snow}{}^4 \qquad (A4)$$

where SVF is sky view factor (dimensionless), TVF is trunk view factor (dimensionless), σ is Stefan-Boltzmann constant ($\sigma \ = \ 5.67 \ \times \ 10^{-8} \mathrm{Wm}^{-2} \mathrm{K}^{-4}$), ε_{sky}, ε_{can}, and ε_{snow} are emissivity coefficients (dimensionless) for sky, canopy, and snow, respectively, and T_{air}, T_{crown}, T_{trunk} and T_{snow} are air, crown, trunk, and snow temperatures (K), respectively. Based on the observed temperatures from *Pomeroy et al.* [2009], a temperature difference, proportional to the insolation amount, is assumed between canopy and air temperatures. Snow temperature is set to air dew point temperature (T_{dp}), when $T_{dp} < 0$ and zero otherwise [*Andreas*, 1986]. Sky emissivity (ε_{sky}) is estimated using the Prata-Kimbal model suggested by *Flerchinger et al.* [2009]. Evaluation of the three shortwave radiation components from equation (4) is relatively complex. Taking into account the infinitely many reflections of shortwave radiation between snow-covered forest floor and canopy [*Bohren and Thorud*, 1973], direct shortwave radiation on the forest floor is evaluated based on a probabilistic approach [*Nilson*, 1971] using the equation [*Essery et al.*, 2008; *Kreith and Kreider*, 2011]

$$\downarrow S_{dir} \ = \ \frac{S_{extr} \ \tau_b \ \cos(\theta) \ e^{-G \lambda L_{path}}}{1 \ - \ \alpha_{dir} \alpha_c (1 \ - \ SVF)} \qquad (A5)$$

where S_{extr} is extraterrestrial solar radiation (Wm^{-2}), τ_b is the atmospheric transmittance for beam radiation (dimensionless), θ is solar incidence angle (the angle between sun and normal to the surface), G is the projection coefficient of leaves orientation (dimensionless), λ is the effective foliage density (m^{-1}), L_{path} is path length of solar beam through canopy (m), α_c is canopy albedo (dimensionless), and α_{dir} is snow albedo for direct radiation (dimensionless). Assuming randomly oriented leaves, G is set to 0.5 and independent on solar angle [*Essery et al.*, 2008]. Diffuse shortwave radiation is calculated based on

$$\downarrow S_{dif} \ = \ \frac{SVF \ S_{extr} \ \tau_d \ \sin\alpha \ \cos^2(\beta/2)}{1 \ - \ \alpha_{dif} \alpha_c (1 \ - \ SVF)} \qquad (A6)$$

where β is the slope angle, τ_d is the atmospheric diffusion factor (dimensionless), and α_{dif} is snow albedo for diffuse

radiation (dimensionless). In this analysis, α_c, α_{dir}, and α_{dif} are set to 0.2 [*Bohren and Thorud*, 1973; *Eck and Deering*, 1990, 1992], 0.4 [*Wiscombe and Warren*, 1980], and 0.8 [*Wang and Zeng*, 2010], respectively. τ_d and τ_b were extracted from the modeled NREL data for the study site. Reflecting shortwave radiation from snow is calculated using [*Hardy et al.*, 1997; *Hardy et al.*, 2004; *Todhunter et al.*, 1992]

$$\uparrow S_{snow} \ = \ \alpha_{dif} \downarrow S_{dif} \ + \ \alpha_{dir} \downarrow S_{dir} \qquad (A7)$$

[30] In absence of any data regarding the spatial distribution of litter and its effects on subcanopy albedo for a range of vegetation densities and tree morphometry, snow albedos (α_{dir} and α_{dif}) are assumed to be spatially uniform, in this study.

Reference

Arbor Day Foundation (2012), ArborDayFoundation-Tree Details—The Tree Guide at arborday.org, Arbor Day Foundation, http://www.arborday.org/.

Andreas, E. L. (1986), A New method of measuring the snow-surface temperature, *Cold Reg. Sci. Technol.*, *12*(2), 139–156.

Anjin, C., K. Yongmin, K. Yongil, and E. Yangdam (2012), Estimation of individual tree biomass from airborne lidar data using tree height and crown diameter, *Disaster Adv.*, *5*(4), 360–365.

Bohren, C. F., and D. B. Thorud (1973), Two theoretical models of radiation heat-transfer between forest trees and snowpacks, *Agric. Meteorol.*, *11*(1), 3–16.

Breidenbach, J., B. Koch, G. Kandler, and A. Kleusberg (2008), Quantifying the influence of slope, aspect, crown shape and stem density on the estimation of tree height at plot level using lidar and InSAR data, *Int. J. Remote Sens.*, *29*(5), 1511–1536.

Cao, Q. V., and T. J. Dean (2011), Modeling crown structure from LiDAR data with statistical distributions, *For. Sci.*, *57*(5), 359–364.

Chavez, V., and S. E. Macdonald (2010), The influence of canopy patch mosaics on understory plant community composition in boreal mixedwood forest, *For. Ecol. Manage.*, *259*(6), 1067–1075.

Eck, T. F., and D. W. Deering (1990), Canopy albedo and transmittance in a boreal forest, *Remote Sens. Sci. Nineties*, *1–3*, 883–886.

Eck, T. F., and D. W. Deering (1992), Canopy albedo and transmittance in a spruce-hemlock forest in mid-September, *Agr. Forest. Meteorol.*, *59*(3–4), 237–248.

Essery, R., P. Bunting, J. Hardy, T. Link, D. Marks, R. Melloh, J. Pomeroy, A. Rowlands, and N. Rutter (2008), Radiative transfer modeling of a coniferous canopy characterized by airborne remote sensing, *J. Hydrometeorol.*, *9*(2), 228–241.

Falkowski, M. J., A. M. S. Smith, A. T. Hudak, P. E. Gessler, L. A. Vierling, and N. L. Crookston (2006), Automated estimation of individual conifer tree height and crown diameter via two-dimensional spatial wavelet analysis of lidar data, *Can. J. Remote Sens.*, *32*(2), 153–161.

Flerchinger, G. N., W. Xaio, D. Marks, T. J. Sauer, and Q. Yu (2009), Comparison of algorithms for incoming atmospheric long-wave radiation, *Water Resour. Res.*, *45*, W03423, doi:10.1029/2008WR007394.

Gatziolis, D., J. S. Fried, and V. S. Monleon (2010), Challenges to estimating tree height via LiDAR in closed-canopy forests: A parable from western oregon, *For. Sci.*, *56*(2), 139–155.

Gaulton, R., and T. J. Malthus (2010), LiDAR mapping of canopy gaps in continuous cover forests: A comparison of canopy height model and point cloud based techniques, *Int. J. Remote Sens.*, *31*(5), 1193–1211.

Gilman, E. F., and D. G. Watson (1994), Picea glauca, USFS Fact Sheet ST-450, http://hort.ufl.edu/database/documents/pdf/tree_fact_sheets/picglaa.pdf (Accessed online, Feb. 2013).

Gryning, S. E., E. Batchvarova, and H. A. R. De Bruin (2001), Energy balance of a sparse coniferous high-latitude forest under winter conditions, *Boundary Layer Meteorol.*, *99*(3), 465–488.

Hanson, J. J., and C. G. Lorimer (2007), Forest structure and light regimes following moderate wind storms: Implications for multi-cohort management, *Ecol. Appl.*, *17*(5), 1325–1340.

Hardy, J. P., R. E. Davis, R. Jordan, X. Li, C. Woodcock, W. Ni, and J. C. McKenzie (1997), Snow ablation modeling at the stand scale in a boreal jack pine forest, *J. Geophys. Res.*, *102*(D24), 29,397–29,405.

Hardy, J. P., R. Melloh, G. Koenig, D. Marks, A. Winstral, J. W. Pomeroy, and T. Link (2004), Solar radiation transmission through conifer canopies, *Agr. Forest. Meteorol.*, *126*(3–4), 257–270.

Hosoi, F., and K. Omasa (2012), Estimation of vertical plant area density profiles in a rice canopy at different growth stages by high-resolution portable scanning lidar with a lightweight mirror, *ISPRS J. Photogramm.*, *74*, 11–19.

Kato, A., L. M. Moskal, P. Schiess, M. E. Swanson, D. Calhoun, and W. Stuetzle (2009), Capturing tree crown formation through implicit surface reconstruction using airborne lidar data, *Remote Sens. Environ.*, *113*(6), 1148–1162.

Kimball, B. A., S. B. Idso, and J. K. Aase (1982), A model of thermal radiation from partly cloudy and overcast skies, *Water Resour. Res.*, *18*(4), 931–936.

Kreith, F., and J. F. Kreider (2011), Principles of sustainable energy, xxiii, 855 p., 816 p. of plates pp., CRC Press, Boca Raton, FL.

Lee, A. C., and R. M. Lucas (2007), A LiDAR-derived canopy density model for tree stem and crown mapping in Australian forests, *Remote Sens. Environ.*, *111*(4), 493–518.

Lundquist, J. D., S. E. Dickerson-Lange, J. A. Lutz, and N. C. Cristea (2013), Lower forest density enhances snow retention in regions with warmer winters: A global framework developed from plot-scale observations and modeling, *Water Resour. Res.*, *49*, doi:10.1002/wrcr.20504.

Maine Forest Commissioner (1908), Forest trees of Maine, p. v., Augusta.

Male, D. H., and R. J. Granger (1981), Snow surface energy exchange, *Water Resour. Res.*, *17*(3), 609–627.

Marks, D., and J. Dozier (1979), A clear-sky longwave radiation model for remote alpine areas, *Arch. Meteorol. Geophys. B*, *27*(2–3), 159–187.

National Climatic Data Center (2012), NCDC's Geodata Portal, http://gis.ncdc.noaa.gov/map/cdo/?thm=themeTemp, Accessed July, 2012.

Nilson, T. (1971), A theoretical analysis of the frequency of gaps in plant stands, *Agric. Meteorol.*, *8*, 25–38.

National Renewable Energy Laboratory (2012), National Renewable Energy Laboratory, www.nrel.gov. Accessed February 2013.

Oshio, H., T. Asawa, A. Hoyano, and S. Miyasaka (2012), Detailed reproduction of three-dimensional crown shape and foliage distribution of trees in an urban area using high-resolution airborne LiDAR, *2012 Ieee International Geoscience and Remote Sensing Symposium* (*Igarss*), 6621–6624.

Pascual, C., A. Garcia-Abril, W. B. Cohen, and S. Martin-Fernandez (2010), Relationship between LiDAR-derived forest canopy height and Landsat images, *Int. J. Remote Sens.*, *31*(5), 1261–1280.

plantmaps.com (2012), PlantMaps-Picea glauca—White spruce interactive native range distribution Map with USDA hardiness zones, http://www.plantmaps.com/nrm/picea-glauca-white-spruce-native-range-map.php.

Pluss, C., and A. Ohmura (1997), Longwave radiation on snow-covered mountainous surfaces, *J. Appl. Meteorol.*, *36*(6), 818–824.

Pomeroy, J. W., D. Marks, T. Link, C. Ellis, J. Hardy, A. Rowlands, and R. Granger (2009), The impact of coniferous forest temperature on incoming longwave radiation to melting snow, *Hydrol. Processes*, *23*(17), 2513–2525.

Price, A. G., and T. Dunne (1976), Energy balance computations of snowmelt in a subarctic area, *Water Resour. Res.*, *12*(4), 686–694.

Reifsnyder, W. E., and H. W. Lull (1965), *Radiant Energy in Relation to Forests*, vol. 6, pp. 111, U.S. Dept. of Agriculture, Forest Service; For sale by the Superintendent of Documents, U.S. Govt. Print. Off., Washington.

Riano, D., E. Chuvieco, S. Condes, J. Gonzalez-Matesanz, and S. L. Ustin (2004), Generation of crown bulk density for Pinus sylvestris L. from lidar, *Remote Sens. Environ.*, *92*(3), 345–352.

Seyednasrollah, B., M. Kumar, and T. E. Link (2013), On the role of vegetation density on net snow cover radiation at the forest floor, *J. Geophys. Res. Atmos.*, *118*, 1–16, doi:10.1002/jgrd.50575.

Sicart, J. E., J. W. Pomeroy, R. L. H. Essery, J. Hardy, T. Link, and D. Marks (2004), A sensitivity study of daytime net radiation during snowmelt to forest canopy and atmospheric conditions, *J. Hydrometeorol.*, *5*(5), 774–784.

Sicart, J. E., J. W. Pomeroy, R. L. H. Essery, and D. Bewley (2006), Incoming longwave radiation to melting snow: Observations, sensitivity and estimation in northern environments, *Hydrol. Processes*, *20*(17), 3697–3708.

Stahli, M., T. Jonas, and D. Gustafsson (2009), The role of snow interception in winter-time radiation processes of a coniferous sub-alpine forest, *Hydrol. Processes*, *23*(17), 2498–2512.

Todhunter, P. E., F. Xu, and J. M. Buttle (1992), A model of net radiation over suburban snowpacks, *Atmos. Environ. Part B*, *26*(1), 17–27.

United States Army Corps of Engineers (1956), Snow hydrology; Summary report of the snow investigations, xxv, 437 p., North Pacific Division, Corps of Engineers, U.S. Army, Portland, Or.

Wang, Z., and X. B. Zeng (2010), Evaluation of snow albedo in land models for weather and climate studies, *J. Clim. Appl. Meteorol.*, *49*(3), 363–380.

Wiscombe, W. J., and S. G. Warren (1980), A model for the spectral albedo of snow. 1. Pure snow, *J. Atmos. Sci.*, *37*(12), 2712–2733.